

The magnetic form factor of the neutron

E.E.W. Bruins^{a,b}

^a *Laboratory for Nuclear Science, Massachusetts Institute of Technology,*

77 Massachusetts Avenue, Cambridge, MA 02139, USA

^b *Temporary Address: DESY, Notkestrasse 85, 22607 Hamburg, Germany*

Abstract

A review of neutron form factor measurements is given. We focus on recent measurements of the neutron magnetic form factor G_M^n , and discuss in detail our measurements of this quantity at momentum transfers $Q^2 = 0.1 - 0.6 \text{ (GeV/c)}^2$.

I. NUCLEON FORM FACTORS

In the one photon exchange approximation, the elastic electron – nucleon differential cross section is described by the so-called Rosenbluth formula¹. The expression contains two electromagnetic form factors which depend on the four momentum transfer squared $q_\mu^2 = -Q^2$ in the reaction, only. These form factors, usually called $G_E(Q^2)$ (electric) and $G_M(Q^2)$ (magnetic), can be thought of as the Fourier representation of the electric charge and current distributions in the nucleon. This relation, however, does not hold at realistic Q^2 , where the recoil of the nucleon and relativistic kinematics are non-negligible. In the Breit (or brick wall) frame, which is the kinematical frame in which no energy is transferred, G_E and G_M are proportional to the nucleon charge and current matrix elements, respectively.

In the late 1950s, Hofstadter and collaborators initiated a series of experiments in which the form factors of the proton and the neutron were measured². The proton form factors were obtained from the measurement of the elastic electron–proton ($e - p$) cross sections at

two different kinematics, keeping Q^2 fixed. Since no free neutron targets are available, the neutron form factors were obtained by measuring the quasi-elastic electron–deuteron ($e - d$) cross sections at the same kinematics, and subsequently subtracting the contribution from the proton using the $e - p$ data.

Most measurements of the proton and neutron form factors, even recent ones^{3–5}, have used this very same technique. By now, the proton form factors are conventionally considered to be known accurately: The proton magnetic form factor G_M^p is known with an accuracy of 2 % up to at least $Q^2 = 1$ (GeV/c)². The electric form factor G_E^p is known to about 5 % at best, due to the fact that its numerical value is smaller than G_M^p in the accessible range of momentum transfers. In the most elaborate recent work on neutron form factors from inclusive measurements, Lung *et al.*⁵ have shown that the neutron magnetic form factor G_M^n can be extracted with an accuracy of 10 – 15 % using this method. The neutron electric form factor G_E^n is essentially undetermined, and recent studies⁶ suggest that polarization variables might be more useful for an unambiguous determination of this small quantity.

Several measurements have attempted an accurate determination of G_M^n by employing coincident neutron detection, initiated in 1962 by the measurement of Stein *et al.*⁷. Neutron detection involves a dedicated neutron detector, usually built from scintillating material, and a careful calibration of its detection efficiency. Because of these experimentally non-trivial considerations, the early measurements^{7–10} did not yield both reliable and accurate data, and consequently large systematic uncertainties had to be introduced. Specific problems were the position dependence of the neutron detection efficiency, which was essentially unknown⁸, and the large proton contribution which forced the experimenters to use heavy shielding^{9,11} or to measure only at high momentum transfers¹⁰.

With the advent of high duty cycle electron machines (ELSA (Bonn), MAMI (Mainz), Jefferson Laboratory (Newport News)) accurate determinations of the neutron form factors are considered realistic, which has led to a renewed interest in these quantities.

II. DETERMINATION OF THE NEUTRON MAGNETIC FORM FACTOR

We have determined the magnetic form factor of the neutron, G_M^n , at four different momentum transfers between $Q^2 = 0.1$ and 0.6 (GeV/c)². The goal of the measurement was to minimize the experimental and theoretical uncertainties and to deliver the first accurate determination of the behavior of G_M^n over an appreciable range of Q^2 .

The ratio of neutron and proton yields at quasifree kinematics was measured for the reactions ${}^2\text{H}(e,e'n)$ and ${}^2\text{H}(e,e'p)$ at momentum transfers $Q^2=0.125, 0.255, 0.417$ and 0.605 (GeV/c)² (Kin. I, II, III and IV), detecting the neutron and the proton simultaneously in the same scintillator array, the nucleon detector. The neutron detection efficiency was measured *in situ* with the ${}^1\text{H}(\gamma,\pi^+)n$ reaction. From this, the ratio R of ${}^2\text{H}(e,e'n)$ and ${}^2\text{H}(e,e'p)$ cross sections was determined and used to extract the neutron magnetic form factor G_M^n in a model insensitive approach, resulting in an inaccuracy between 2.1 and 3.3 % in G_M^n .

The method employed, first suggested by Durand¹², was previously applied in only a few experiments^{9,10}. In this way the luminosity, the electron detection efficiency, and the electron solid angle cancel out, while the nucleon acceptances and the choice of the deuteron wave function cancel out to first order. The lay-out of the experiment minimized corrections due to proton losses, and the restriction to quasifree kinematics minimized nuclear effects and their corresponding uncertainties.

The ratio R of the cross sections of the ${}^2\text{H}(e,e'n)$ and ${}^2\text{H}(e,e'p)$ reactions was determined after taking into account proton losses due to nuclear reactions, multiple scattering and edge effects, and an *in situ* calibration of the neutron detection efficiency. G_M^n was extracted taking into account nuclear effects, using the known $e-p$ cross sections and available information on G_E^n . G_E^n contributes less than 2 % to the $e-n$ cross section and is not a dominant source of uncertainty.

A. Experimental details

1. The detector setup

The electron beam (between 900 and 1600 MeV, 20 to 60 nA, 20 to 50 % duty cycle, depending on kinematics), delivered by the ELSA accelerator at the Physics Institute at Bonn, impinged axially on a cylindrical target (length 10 cm) made from 125 μm thick kapton and filled with liquid Hydrogen or Deuterium. Electrons (and pions from the ${}^1\text{H}(\gamma,\pi^+)n$ reaction) were detected in the ELAN magnetic spectrometer with four scintillators and MWPCs and one Čerenkov counter.

Protons and neutrons were detected in the nucleon detector using the time of flight method. Since protons are about hundred times more abundant than neutrons, a reliable particle identification is important. We used three thin veto scintillators which allowed a misidentification rate of far less than 10^{-4} , and the verification of the losses due to pile-up¹³.

For Kinematics I, II and III, the nucleon detector, which was used previously, consisted of a total of five scintillators (NE102a) of dimensions $25 \times 25 \text{ cm}^2$ with a thickness of 2 mm for the ΔE detectors (1 mm for Kin. I) and 50 mm for the E counters. The first E counter (E_{front}) detected simultaneously protons and neutrons, while shielding behind E_{front} prevented protons from the quasielastic ${}^2\text{H}(e,e'p)$ reaction to reach E_{back} . The neutrons detected in E_{back} were used to determine the losses in the neutron yield in E_{front} caused by the software gates on the veto detectors. For Kin. IV, the detectors of dimensions $100 \times 18 \text{ cm}^2$ and thickness 1 cm and 18 cm, respectively, had a two-sided readout. At this large proton energy the use of lead to shield E_{back} becomes impracticable. We therefore installed two veto detectors between E_{front} and E_{back} in order to determine the neutron losses. For a more detailed description, see Ref.¹⁴. Each measurement of R was bracketed by two calibration runs for the neutron detection efficiency. To switch from the calibration to the measurement of the ratio, only the target and the spectrometer settings needed to be changed, which reduced the risk of systematic errors.

B. The analysis

Neutrons detected in the nucleon detector were defined by a signal in E_{front} or in E_{back} at the correct time with respect to the spectrometer and in excess of a certain software adjustable threshold, together with a neutron condition on the veto counters. Different veto conditions on the ADC and TDC information were applied and used for stringent cross checks. Thanks to the duty cycle of the ELSA stretcher ring (20 to 50 %), a signal to noise ratio of 200:1 for neutrons was achieved (Fig. 1).

The stability of the neutron detection efficiency of E_{front} , η_n , was monitored by means of the ADC signal for protons, and by the number of neutrons coming from the ${}^2\text{H}(e,e'n)$ reaction scaled with the number of electrons in the spectrometer. At Kin. III and IV, the ${}^2\text{H}(\gamma,p)n$ reaction served as an additional monitor for the stability of η_n . This reaction can not be used to determine the absolute value of η_n since pion production cannot be excluded.

The reaction ${}^1\text{H}(\gamma,\pi^+)n$ was used to obtain an *in situ*, absolute determination of the detector efficiency for neutrons. Under the assumption that only real photons are used, the kinematics of this reaction can be arranged in such a way as to unambiguously tag neutrons impinging on the nucleon detector centered at the same energy as those from the ${}^2\text{H}(e,e'n)$ reaction. Eighty percent of the pion flux in the spectrometer was determined to actually originate from virtual photons, i.e. from the ${}^1\text{H}(e,\pi^+)e'X$ reaction. Monte Carlo simulations¹⁵, however, show that more than 99 % of the pions which enter the spectrometer (and satisfy the cuts used in the analysis, as described in Ref.¹⁴) originate from electrons scattering to extremely small angles ($\ll 5^\circ$). Because of the stringent requirements put on the pion kinematics, the resulting data set can be treated as originating from the real photon induced ${}^1\text{H}(\gamma,\pi^+)n$ reaction. This consideration is unfortunately not supported by simulations performed by the Basel group, which have recently published competing G_M^n results¹⁶. The discrepancy has to be resolved in the near future. Curiously, for neutrons with an average energy of 61 MeV, the measured detection efficiency in the center of the nucleon detector as a function of threshold agreed with the one established earlier^{13,17}.

In order to obtain R , the measured yields must be corrected for: *i*) the net proton losses due to nuclear reactions and multiple scattering in the material between the reaction vertex and the detector; *ii*) the dependence of the neutron detection efficiency on the distribution of the neutrons in space and energy over the detector surface. Details about the small corrections for Hydrogen contamination of the Deuterium, and for the contributions of the target end caps to the different reactions can be found in Ref.¹⁴. In addition, for an extraction of G_M^n one must evaluate nuclear effects, such as final state interactions (FSI), meson exchange currents (MEC) and isobar currents (IC), which alter the proton and neutron yields expected from free proton respectively neutron targets.

The $^1\text{H}(e,e')\text{p}$ reaction was used for the determination of the proton detection efficiency, including the above mentioned losses. The experimentally found losses were consistent with numerical checks done with the GEANT package¹⁸ which was extended to include total proton cross sections at low energies¹⁹. Protons from the $^1\text{H}(e,e')\text{p}$ and the $^2\text{H}(e,e')\text{n}$ reaction also were used to calibrate and monitor the light response of the scintillators in view of the threshold dependence of the neutron detection efficiency.

The reactions $^2\text{H}(e,e'n)$ and $^1\text{H}(\gamma,\pi^+)\text{n}$ lead to different energy and position distributions of neutrons in E_{front} . While the neutron distribution for the $^1\text{H}(\gamma,\pi^+)\text{n}$ reaction is known from experiment, the $^2\text{H}(e,e'n)$ distribution was obtained using the ENIGMA Monte Carlo code²⁰. The second order effect of the different distributions (including edge effects) on the ratio R was simulated with the program KSUVAX²¹. The response of the detector used for Kin. I, II and III had been calibrated carefully previously²² using a tagged neutron beam at PSI. The positional dependence of the response of the detector used for Kin. IV was studied by means of its double read out system.

C. Nuclear effects

Nuclear effects cause R to differ from the expected ratio R_{free} for free nucleons: $R_{free} = R * (1 - \delta R)$. The corrections δR were calculated in two different models, of which the first²³

includes FSI, MEC and IC, and shows that FSI dominate the other corrections, whereas the second one²⁴ includes only FSI but is fully relativistic. It appears that the result for G_M^n obtained from R is affected to less than 0.4 % by relativistic effects. We use the difference between the two calculations, including FSI only, as an indication of the inherent model uncertainties, and their average as the most probable correct value. To this average, we add then the effects of MEC and IC which are taken as the difference between the full calculation, and the calculation including FSI only, both within the same model²³. We conservatively estimate the uncertainty due to these effects to be half their size. The values of δR range from 2.2 to 8.5 %, depending on the kinematics.

D. Results

For the extraction of G_M^n , the $e - p$ cross sections are needed. The measured cross section data²⁶ have been averaged in small intervals around the central Q^2 values, taking into account the Q^2 dependence obtained from the dipole form factors for the proton ($G_E^p = G_D = (1 + Q^2/a^2)^{-2}$, $G_M^p = 2.793 * G_E^p$, and $a^2 = 0.710$ (GeV/c)²). The statistical errors of the used data points determine the statistical error in the average. In order to obtain the systematical error, the average has been recalculated after each $e - p$ data set had been changed individually by its systematical errors, and adding the resulting changes quadratically. G_E^n was chosen to be 0.037 ± 0.017 ²⁷.

The results for G_M^n are shown in Fig. 2. We confirm our pilot measurement at $Q^2 = 0.125$ (GeV/c)², performed at the MEA accelerator (NIKHEF, Amsterdam) with the same nucleon detector as used in Kin. I, II and III. Note that the *published* results differ by more than one standard deviation, only because of the difference in the value for the proton cross section used. This difference, 2 %, comes from the different Q^2 range of the $e - p$ data used in the fit and reflects our knowledge of the $e - p$ cross section. Our value for G_M^n at this momentum transfer is significantly higher than our previous result for $Q^2 = 0.093$ (GeV/c)² obtained at MEA. Fig. 2 suggests a slope in G_M^n/G_D around these momentum transfers.

Recently Markowitz et al.¹¹ determined G_M^n from an absolute measurement of the ${}^2\text{H}(e,e'n)$ cross section. At 0.109 (GeV/c)^2 , their result lies 13.6 % above the dipole fit, whereas our result at 0.125 (GeV/c)^2 is only 2.5 % above. Relativistic effects, which have not been applied in Ref.¹¹, do not appear to remove this discrepancy. Our results agree with the other results of Markowitz, and with the result obtained by Gao²⁵ using polarisation techniques. Fig. 2 shows that most of the recent theoretical predictions of G_M^n are not in agreement with our data. We only show some of the (rare) theoretical predictions which are not fits to G_M^n data. The only model which reproduces the trend indicated by the data is the minimal model of Meissner²⁸. Since Meissner's *complete* model does not reproduce the suggested trend, we observe that none of the parameter-free models presently available describes the trend in G_M^n as observed in our data. The data show for the first time a significant violation of the scaling rule $G_M^p/\mu_p = G_M^n/\mu_n$.

III. CONCLUSIONS AND OUTLOOK

We have combined the ratio method proposed long ago with the possibilities offered only recently by the large duty cycle electron beams to measure G_M^n with substantially decreased uncertainties. The coincident detection of the electron and the knocked out nucleon reduces significantly uncertainties due to nuclear effects, whereas the large duty cycle allows to detect simultaneously protons and neutrons.

Recently, a new set of data has become available from the MAMI accelerator, Mainz¹⁶ covering a similar range in momentum transfer. Although these data confirm the violation of the above mentioned scaling rule, they differ significantly from our results. This fact is under investigation, and a possible explanation has been given in section IIB.

An experiment has been approved at the Bates accelerator, in which G_M^n will be measured at small Q^2 , i.e. $< 0.125 \text{ (GeV/c)}^2$, using the method as employed by Ref.¹¹. Although nuclear effects are large for the proposed measurement, the result will be a continuous set of data points up to the region where the existence of a sudden fluctuation in G_M^n has been

claimed¹¹.

At TJNAF, an experiment has been approved in which G_M^n will be measured using the ratio method at $Q^2 = 0.3 - 5.1$ (GeV/c)². One of the main experimental problems in this experiment will be the matching of the proton and neutron phase spaces, due to the different techniques employed to detect each of the nucleons.

REFERENCES

- ¹ M. Rosenbluth, Phys. Rev. **79** (1950) 615
- ² C. de Vries *et al.*, Phys. Rev. **134B** (1964) 848
- ³ S. Rock *et al.*, Phys. Rev. Lett. **49** (1982) 1139
- ⁴ R. G. Arnold *et al.*, Phys. Rev. Lett. **61** (1988) 806
- ⁵ A. Lung *et al.*, Phys. Rev. Lett. **70** (1993) 718
- ⁶ M. Meyerhoff *et al.*, Phys. Lett. **B327** (1994) 201; J. Becker, Proc. 12th Int. Symp. on High-Energy Spin Physics (1996), to be published
- ⁷ P. Stein *et al.*, Phys. Rev. Lett. **9** (1962) 403
- ⁸ P. Stein *et al.*, Phys. Rev. Lett. **16** (1966) 592
- ⁹ W. Bartel *et al.*, Phys. Lett. **30B**, 285 (1969)
- ¹⁰ W. Bartel *et al.*, Phys. Lett. **39B**, 407 (1972)
- ¹¹ P. Markowitz *et al.*, Phys. Rev. **C48**, R5 (1993)
- ¹² L. Durand, Phys. Rev. **115**, 1020 (1959); **123**, 1393 (1961)
- ¹³ F. C. P. Joosse, Ph.D. Thesis, Universiteit Utrecht (1993); D. Fritschi, Ph.D. Thesis, Universität Basel (1993)
- ¹⁴ E. E. W. Bruins, Ph.D. Thesis, Universiteit Utrecht (1995)
- ¹⁵ H. Reike, Ph.D. Thesis, Universität Bonn (1993); priv. comm.
- ¹⁶ J. Jourdan, this workshop; priv. comm.
- ¹⁷ H. Anklin *et al.*, Phys. Lett. **B336**, 313 (1994)
- ¹⁸ CERN Computer Newsletter **200**, 13 (1990)

- ¹⁹ Z. Papandreou, Int. Rep., Universiteit Utrecht (1992)
- ²⁰ J.L.Visschers, in: MC93, edited by P. Dragovitsch, S. L. Linn, and M. Burbank, World Scientific Publ. Co. (1994) p. 350
- ²¹ R. A. Cecil, B. D. Anderson and R. Madey, Nucl. Instr. Meth. **161**, 439 (1979)
- ²² M. Loppacher, Diplomarbeit, Universität Basel (1992)
- ²³ H. Arenhövel, W. Leidemann and E. L. Tomusiak, Phys. Rev. **C46**, 455 (1992)
- ²⁴ E. Hummel and J. A. Tjon, Phys. Rev. **C49**, 21 (1994)
- ²⁵ H. Gao et al., Phys. Rev. **C50**, R546 (1994)
- ²⁶ data compilation by J. Jourdan (priv. comm.)
- ²⁷ S. Platchkov et al., Nucl. Phys. **A510**, 740 (1990)
- ²⁸ U.-G. Meissner, Phys. Rep. **161** Nos. 5 & 6, 213 (1988) (1994)
- ²⁹ M. Warns et al., Z. Phys. **C45** 627 (1990)
- ³⁰ F. Schlumpf, J. Phys. G: Nucl. Part. Phys. **20** 237 (1994)

FIGURES

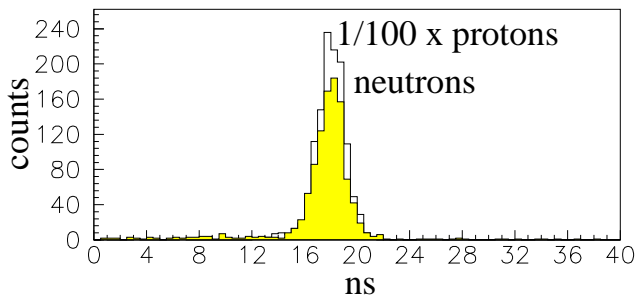


FIG. 1. Time spectra of protons (line) and neutrons (shaded area) using a subset of the data from the measurement at $Q^2=0.255$ (GeV/c) 2 .

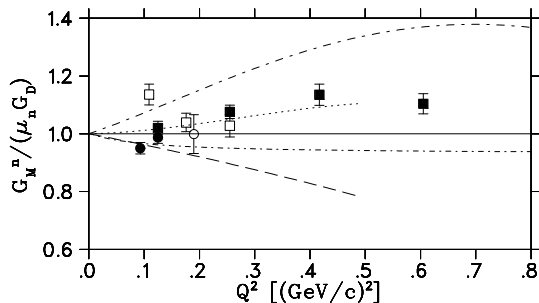


FIG. 2. Data from recent G_M^n measurements up to $Q^2=0.8$ (GeV/c) 2 , scaled to the dipole fit: black circles [17], open squares [11], open circle [25]. The black squares are from this work. Several model predictions are shown. VMD: The minimal (dotted line) and complete (long dash) model of [28]. Constituent Quark Model: non-relativistic calculation of [29] (dot-long dash), relativistic calculation of [30] (dot-short dash).